

Periodic bouncing modes for two uniformly magnetized spheres I: Trajectories

Boyd F. Edwards and Bo A. Johnson

*Department of Physics
Utah State University
Logan, UT 84322*

John M. Edwards

*Department of Computer Science
Utah State University
Logan, UT 84322*

(Dated: August 21, 2019)

We consider a uniformly magnetized sphere that moves without friction in a plane in response to the field of a second, identical, fixed sphere, making elastic hard-sphere collisions with this sphere. We seek periodic solutions to the associated nonlinear equations of motion. We find closed-form mathematical solutions for small-amplitude modes, and use these to characterize and validate our large-amplitude modes, which we find numerically. Our Runge-Kutta integration approach allows us to find 1,243 distinct periodic modes with the free sphere located initially at its stable equilibrium position. Each of these modes bifurcates from the finite-amplitude radial bouncing mode with infinitesimal-amplitude angular motion, and supports a family of states with increasing amounts of angular motion. These states offer a rich variety of behaviors and beautiful, symmetric trajectories, including states with up to 157 collisions and 580 angular oscillations per period.

A vibrant online learning community shares information about building beautiful sculptures from collections of small neodymium magnet spheres, with YouTube tutorial videos attracting over a hundred million views [1, 2]. These spheres offer engaging hands-on exposure to principles of magnetism, and are used both in and out of the classroom to teach principles of mathematics, physics, chemistry, biology, and engineering [3]. We showed recently that the forces and torques between two uniformly magnetized spheres are identical to the forces and torques between two point magnetic dipoles. In the present paper, we exploit this equivalence to study the nonlinear dynamics of a uniformly magnetized sphere subject to the magnetic forces and torques produced by a second, fixed, uniformly magnetized sphere, assuming hard-sphere elastic collisions between them. Our search for periodic states uncovers a wide variety of periodic modes, some of which are highly complex and beautiful.

I. INTRODUCTION

Scientific investigations of the behavior of collections of spherical magnets include studies of chain, ring, and tube formation [4–6], a continuum model for magnet chain energy [7], mechanical properties of chains and cylinders [8], stable defects along chains and rings [9], eigenmodes for lateral oscillations of a straight chain [10], stability of vertical chains [11], and radiation damping for two magnets oscillating in each other’s fields [12]. These studies

emphasize the energetics and stability of symmetric assemblies of many spherical magnets.

A single uniformly magnetized sphere can exhibit complex motions as it responds to the forces and torques exerted by a fixed but otherwise identical sphere. We recently studied the motion of a free sphere that slides without friction along the surface of a fixed sphere, with orbital and spin degrees of freedom for the free sphere but no radial motion. These assumptions give periodic nonlinear states and infinite cascades of mixed-mode bifurcations [13].

In the present paper, we study the motion of a free sphere that makes contact with a fixed sphere only during elastic hard-sphere collisions, and we therefore include orbital, spin, and radial degrees of freedom for the free sphere. Compared with our previous study of periodic sliding states, adding the radial degree of freedom means that three degrees of freedom must be synchronized instead of two in order to find periodic solutions.

We locate the free sphere initially at its stable equilibrium position, with its south pole in direct contact with the north pole of the fixed sphere, and we search for periodic states by varying the initial orbital, spin, and radial momenta.

We find closed-form periodic solutions for small-amplitude motion near this equilibrium position, solutions that are characterized by the number m of bounces per period, the number of angular oscillations n per period, and the phase relationship p between the orbital and spin motions.

We find finite-amplitude modes numerically, using (m, n, p) to characterize these modes, and validating our simulation code by comparison with our closed-form

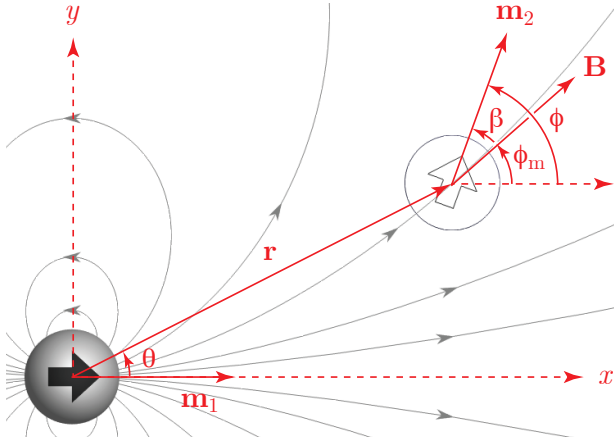


Figure 1. Polar coordinates (r, θ) used to describe the 2D position of a free sphere with magnetic dipole moment \mathbf{m}_2 , whose direction is given by the angle ϕ , measured counterclockwise from the $+x$ direction. This sphere moves in response to the forces and torques produced by a sphere that is held fixed at the origin, with its magnetic moment \mathbf{m}_1 fixed in the $+x$ direction and its magnetic field lines shown as directed traces. At the position \mathbf{r} of the free sphere, ϕ_m gives the direction of the local magnetic field \mathbf{B} and β gives the direction of \mathbf{m}_2 relative to \mathbf{B} .

small-amplitude results. This search yields 1,243 distinct and highly varied modes. The bulk of the paper is devoted to characterizing and understanding these modes.

We take advantage of our recent proof that simple dipolar interactions exactly describe the magnetic interactions between uniformly magnetized spheres [14, 15]. In a companion paper, we explore scaling relationships for the energy and period of periodic modes discussed in the present paper [16].

II. MATHEMATICAL DESCRIPTION

We describe the 2D position of the free sphere using polar coordinates (r, θ) , and describe its magnetic orientation by ϕ (Fig. 1). The corresponding radial momentum p_r , orbital angular momentum p_θ , and spin angular momentum p_ϕ bring the state-space dimensionality to six, and energy conservation supplies an algebraic relationship between these six dynamical variables that reduces the effective dimensionality to five.

For a magnetic sphere of radius a with uniform magnetization \mathbf{M} , the total magnetic dipole moment is

$$\mathbf{m}_1 = \frac{4}{3}\pi a^2 \mathbf{M}. \quad (1)$$

Placing this dipole at the coordinate origin (Fig. 1) produces a pure dipole magnetic field given by

$$\mathbf{B}(\mathbf{r}) = \frac{\mu_0}{4\pi} \left(\frac{3\mathbf{m}_1 \cdot \mathbf{r}}{r^5} \mathbf{r} - \frac{\mathbf{m}_1}{r^3} \right), \quad (2)$$

where $\mathbf{B}(\mathbf{r})$ is the magnetic field of the fixed sphere at the position \mathbf{r} of the free sphere, of magnitude $r > a$.

The potential energy, force, and torque on the free sphere are the same as those for a point dipole, and are given respectively by [14]

$$U = -\mathbf{m}_2 \cdot \mathbf{B}, \quad (3)$$

$$\mathbf{F} = -\nabla U, \quad (4)$$

$$\boldsymbol{\tau} = \mathbf{m}_2 \times \mathbf{B}. \quad (5)$$

The potential energy U is lowest where \mathbf{B} is strong and where \mathbf{m}_2 is aligned with \mathbf{B} . The force \mathbf{F} on the free sphere is directed toward such regions, assuming that \mathbf{m}_2 is fixed in direction, and the torque $\boldsymbol{\tau}$ tends to rotate the free sphere in order to align \mathbf{m}_2 with \mathbf{B} .

The free and fixed spheres have identical radii a , dipole moment magnitudes $|\mathbf{m}_1| = |\mathbf{m}_2| = \hat{m}$, masses \tilde{m} , and moments of inertia $I = 2\tilde{m}a^2/5$ (Fig. 1). The fixed sphere is placed at the origin, and has fixed magnetic moment $\mathbf{m}_1 = \hat{m}\hat{\mathbf{x}}$. The free sphere is located at

$$\mathbf{r} = r \cos \theta \hat{\mathbf{x}} + r \sin \theta \hat{\mathbf{y}}, \quad (6)$$

and its dipole moment is given by

$$\mathbf{m}_2 = \hat{m} \cos \phi \hat{\mathbf{x}} + \hat{m} \sin \phi \hat{\mathbf{y}}. \quad (7)$$

This dipole moment is oriented at an angle ϕ measured counterclockwise from the $+x$ direction (Fig. 1).

Equation (2) supplies the Cartesian components of the magnetic field at the center of the free sphere [13],

$$\mathbf{B}(\mathbf{r}) = \frac{\mu_0 \hat{m}}{8\pi r^3} \left[(1 + 3 \cos 2\theta) \hat{\mathbf{x}} + 3 \sin 2\theta \hat{\mathbf{y}} \right]. \quad (8)$$

The direction of this field is given by

$$\phi_m(\theta) = \tan^{-1} \left(\frac{3 \sin 2\theta}{1 + 3 \cos 2\theta} \right), \quad (9)$$

measured counterclockwise from the $+x$ direction. The magnetic displacement angle β is defined as the angle between \mathbf{m}_2 and $\mathbf{B}(\mathbf{r})$ (Fig. 1),

$$\beta = \phi - \phi_m(\theta). \quad (10)$$

If \mathbf{m}_2 points in the direction of \mathbf{B} , then $\beta = 0$ and $\boldsymbol{\tau} = 0$. If \mathbf{m}_2 and \mathbf{B} are misaligned, then $\beta \neq 0$ and the torque $\boldsymbol{\tau}$ attempts to align \mathbf{m}_2 with \mathbf{B} .

Using dimensionless variables, the Hamiltonian and

dynamical equations become [13]

$$E = \frac{p_r^2}{2} + \frac{p_\theta^2}{2r^2} + 5p_\phi^2 - \frac{1}{12r^3} [\cos \phi + 3\cos(\phi - 2\theta)] \quad (11a)$$

$$\dot{r} = p_r \quad (11b)$$

$$\dot{\theta} = \frac{p_\theta}{r^2} \quad (11c)$$

$$\dot{\phi} = 10p_\phi \quad (11d)$$

$$\dot{p}_r = \frac{p_\theta^2}{r^3} - \frac{1}{4r^4} [\cos \phi + 3\cos(\phi - 2\theta)] + F_N \quad (11e)$$

$$\dot{p}_\theta = \frac{1}{2r^3} \sin(\phi - 2\theta) \quad (11f)$$

$$\dot{p}_\phi = -\frac{1}{12r^3} [\sin \phi + 3\sin(\phi - 2\theta)], \quad (11g)$$

where a normal force F_N is exerted by the fixed sphere on the free sphere when they are in contact.

As is readily seen from these equations, the free sphere finds a stable equilibrium position at $(r, \theta, \phi) = (1, 0, 0)$, with $p_r = p_\theta = p_\phi = 0$ and $E = -1/3$. This corresponds to orienting the magnetic moments of the two spheres along the line joining their centers, with the south pole of the free sphere in contact with the north pole of the fixed sphere. Below, we seek initial values of p_r , p_θ , and p_ϕ that yield periodic states, with the free sphere located initially at the stable equilibrium position.

III. SMALL-AMPLITUDE PERIODIC STATES

In this section, we find small-amplitude periodic states in the vicinity of the stable equilibrium position, with synchronized radial, orbital, and spin motions. These states serve as a guide to our investigations of finite-amplitude periodic states, and serve to validate our numerical results.

A. Radial Motion

We first consider small-amplitude radial motion along the x axis. We accordingly set $r(t) = 1 + \epsilon(t)$ and $\theta = \phi = p_\theta = p_\phi = 0$ in Eqs. (11) to find

$$E = -\frac{1}{3} + \epsilon + \frac{\dot{\epsilon}^2}{2} \quad (12a)$$

$$\ddot{\epsilon} = -1. \quad (12b)$$

These equations are valid when the spheres are not in contact ($\epsilon > 0$), and for small ϵ . Thus, the free sphere experiences constant acceleration $\ddot{r} = \ddot{\epsilon} = -1$ directed toward the fixed sphere, like a particle moving under gravity near the earth's surface. We seek a relationship between the energy E and the period T_r of small-amplitude radial bouncing motions, with each bounce being a hard-sphere instantaneous elastic collision of the free sphere

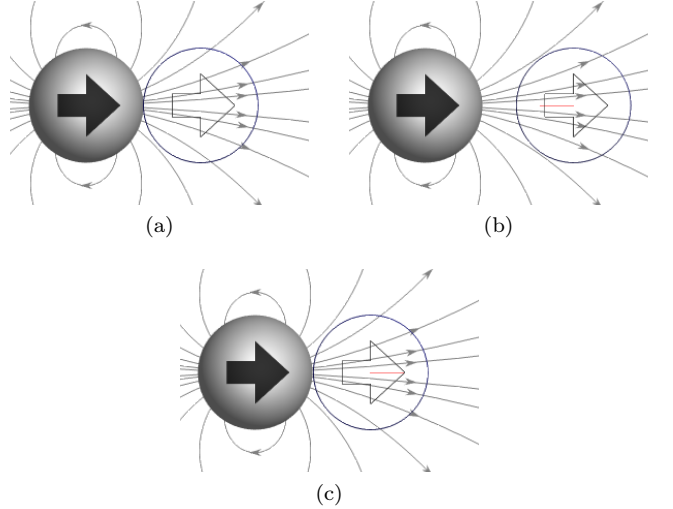


Figure 2. *MagPhyx* snapshots of the radial bouncing mode discussed in Sec. III A [17]. The shaded sphere is fixed in position and orientation, and the outlined sphere bounces periodically on the fixed sphere. Arrows superposed over the spheres give the directions of their magnetic moments. Magnetic field lines are shown as grey traces, and the path of the motion of the free sphere is shown as a red trace.

with the fixed sphere. To do so, we impose the initial conditions $\epsilon(0) = 0$ and $\dot{\epsilon}(0) = v_0$, which apply immediately after the free sphere collides with the fixed sphere. In this way, the period T_r is the time elapsed until the next collision. Integrating Eq. (12b) yields

$$\epsilon(t) = v_0 t - \frac{1}{2} t^2. \quad (13)$$

Substituting Eq. (13) into Eq. (12a) gives the conserved total energy,

$$E = -\frac{1}{3} + \frac{v_0^2}{2}. \quad (14)$$

Setting $\epsilon(t) = 0$ in Eq. (13) at time $t = T_r$ gives the period of the bouncing motion,

$$T_r = 2v_0. \quad (15)$$

Combining Eqs. (14) and (15) gives the desired relationship between the energy and the period,

$$E = -\frac{1}{3} + \frac{T_r^2}{8} \quad (16)$$

$$T_r = \sqrt{8 \left(E + \frac{1}{3} \right)}. \quad (17)$$

Figure 2 illustrates this mode, and *MagPhyx*, Demo 1 visualizes it [17]. In this mode, the free sphere bounces periodically on the fixed sphere, with \mathbf{m}_2 always aligned with \mathbf{B} . Thus, the potential energy is associated with movement of the sphere into regions of weaker magnetic fields \mathbf{B} .

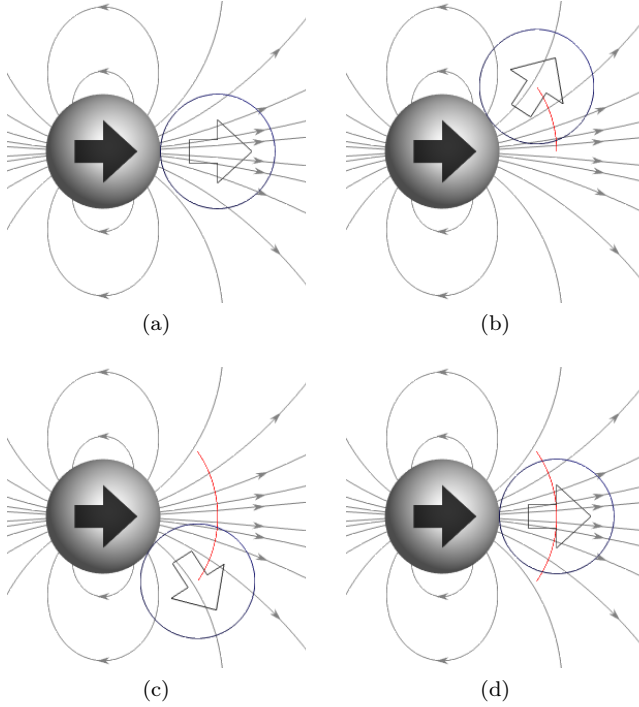


Figure 3. *MagPhyx* snapshots of the in-phase angular sliding mode discussed in Sec. III B (mode 1), with orbital motion dominating over spin motion.

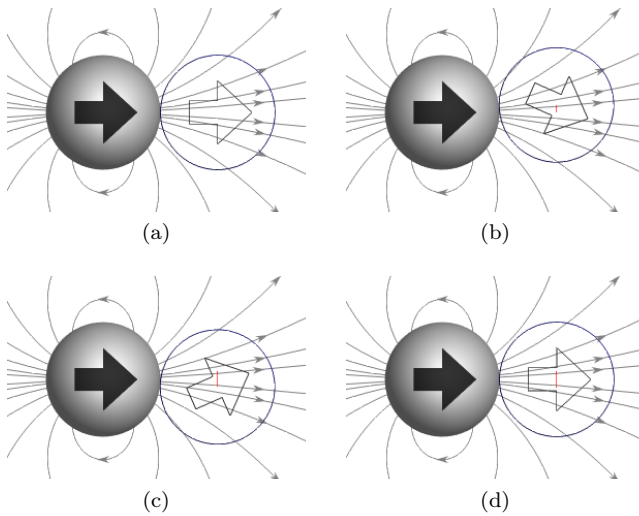


Figure 4. *MagPhyx* snapshots of the out-of-phase angular sliding mode discussed in Sec. III B (mode 2), with spin motion dominating over orbital motion.

B. Angular Motion

In this section, we describe small-amplitude spin and orbital oscillations of the free sphere about the stable equilibrium position, with no radial motion and with the free sphere maintaining frictionless contact with the fixed sphere ($r = 1$ and $p_r = 0$). To first order in θ and ϕ ,

Eqs. (11) give

$$\begin{pmatrix} \ddot{\theta} \\ \ddot{\phi} \end{pmatrix} = \begin{pmatrix} -1 & 1/2 \\ 5 & -10/3 \end{pmatrix} \begin{pmatrix} \theta \\ \phi \end{pmatrix}, \quad (18a)$$

and Eqs. (9) and (10) give

$$\beta = \phi - \frac{3}{2}\theta. \quad (18b)$$

We seek normal modes for which θ , ϕ , and β oscillate at the same angular frequency ω , of the form

$$\theta(t) = Ce^{i\omega t} \quad (19a)$$

$$\phi(t) = De^{i\omega t} \quad (19b)$$

$$\beta(t) = Ee^{i\omega t}, \quad (19c)$$

where C , D , and E are constants.

Equations (18) yield two normal modes. The lowest-frequency mode has an angular frequency ω_1 given by

$$\omega_1^2 = \frac{13 - \sqrt{139}}{6}, \quad (20)$$

period

$$T_1 = \frac{2\pi}{\omega_1} \approx 14, \quad (21)$$

and phase relationships

$$\phi_1 = 2(1 - \omega_1^2)\theta_1 \quad (22a)$$

$$\approx 1.6\theta_1 \quad (22b)$$

and

$$\beta_1 = \left(\frac{1}{2} - 2\omega_1^2\right)\theta_1 \quad (23a)$$

$$\approx 0.097\theta_1. \quad (23b)$$

Because θ_1 and ϕ_1 have the same sign, the orbital and spin oscillations are in phase. Because $|\beta_1| \ll |\theta_1|$, the magnetic moment \mathbf{m}_2 stays closely aligned with the local magnetic field \mathbf{B} as the free sphere slides back and forth against the fixed sphere [13]. Thus, the potential energy is dominated by orbital movement of the sphere into regions of weaker magnetic fields \mathbf{B} . Figure 3 illustrates this mode at a finite amplitude, and *MagPhyx*, Demo 11 visualizes it [17].

The other mode has larger angular frequency ω_2 , given by

$$\omega_2^2 = \frac{13 + \sqrt{139}}{6}, \quad (24)$$

smaller period

$$T_2 = \frac{2\pi}{\omega_2} \approx 3.1, \quad (25)$$

and phase relationships

$$\phi_2 = 2(1 - \omega_2^2) \theta_2 \quad (26a)$$

$$\approx -6.3 \theta_2 \quad (26b)$$

and

$$\beta_2 = \left(\frac{1}{2} - 2\omega_2^2 \right) \theta_2 \quad (27a)$$

$$\approx -7.8 \theta_2. \quad (27b)$$

Because θ_2 and ϕ_2 have opposite signs, the orbital and spin oscillations are 180° out of phase. Because $|\beta_2| \gg |\theta_2|$, the direction of \mathbf{m}_2 departs significantly from the direction of \mathbf{B} , but the free sphere remains close to its equilibrium position as it slides against the fixed sphere [13]. Thus, the potential energy is dominated by spin misalignment of \mathbf{m}_2 with \mathbf{B} rather than with movement of the free sphere into regions of weaker magnetic fields \mathbf{B} . Figure 4 illustrates this mode at finite amplitude, and *MagPhyx*, Demo 12 visualizes it [17].

C. Radial and Angular Motion

In this section, we describe periodic states with small-amplitude radial and angular oscillations about the stable equilibrium position. These states can be constructed by combining the small-amplitude motions discussed in the previous two subsections, noting that the period T_r of the radial motion [Eq. (17)] depends on energy, with $T_r \rightarrow 0$ as $E \rightarrow -1/3$. Since the periods T_1 and T_2 of the in-phase and out-of-phase angular motions [Eqs. (21) and (25)] do not depend on energy, we can take advantage of the energy dependence of T_r to find values of the energy for which the radial motion synchronizes with the angular motion.

For orbital and spin oscillations that are in phase with each other, we can synchronize angular and radial oscillations by writing the period of the overall motion as $T = mT_r = nT_1$, with a bouncing number m giving the number of bounces per period and a rocking number n giving the number of angular oscillations per period. We designate these in-phase modes by $(m, n, 1)$.

For orbital and spin oscillations that are out of phase with each other, we can synchronize angular and radial oscillations by writing the period of the overall motion as $T = mT_r = nT_2$, with m and n defined as before. We designate these out-of-phase modes by $(m, n, 2)$.

We designate modes generally by (m, n, p) , with $p = 1$ for in-phase modes and $p = 2$ for out-of-phase modes. Writing the period as $T = mT_r = nT_p$ and applying Eq. (16) yields the small-amplitude energy and period, valid for $m \gg n$,

$$E_{mnp} = -\frac{1}{3} + \frac{n^2 T_p^2}{8m^2} \quad (28)$$

$$T_{mnp} = nT_p, \quad (29)$$

where T_1 and T_2 are given by Eqs. (21) and (25), respectively.

We have just shown that small-amplitude periodic states have large bouncing numbers m compared with their rocking numbers n . In these states, the bouncing frequency is high and the free sphere remains in close proximity to the fixed sphere.

Thus, there are two types of small-amplitude periodic states involving both radial and angular motion, one whose angular motion is dominated by orbital motion, with orbital and spin oscillations that are in phase ($p = 1$), and the other whose angular motion is dominated by spin motion, with orbital and spin oscillations that are out of phase ($p = 2$). The energies and periods of both types of states are given by Eqs. (28) and (29), with m giving the number of bounces per period and n giving the number of angular oscillations per period.

IV. FINITE-AMPLITUDE PERIODIC STATES

We seek periodic motions of the free sphere with initial position $r(0) = 1$, $\theta(0) = 0$, $\phi(0) = 0$ and initial nonzero momenta $p_r(0) > 0$, $p_\theta(0)$, and $p_\phi(0)$. These initial conditions place the free sphere at the stable equilibrium position, with its magnetic moment aligned with the fixed sphere, and endow the sphere with nonzero radial momentum, orbital angular momentum, and spin angular momentum. Taking $p_r(0) > 0$ means that, at the initial time, the free sphere has just completed a hard-sphere collision with the fixed sphere. Given that the initial position of the free sphere is always the same, it is the values of the initial momenta $p_r(0)$, $p_\theta(0)$, and $p_\phi(0)$ that completely determine the subsequent motion of the sphere.

Because $E = -1/3$ is a minimum, and because states with $E \geq 0$ are unbounded [13], we seek periodic states with $-1/3 < E < 0$. Finding a particular mode (m, n, p) is guaranteed only for $m \gg n$, for which Eqs. (28) and (29) pertain for small amplitudes.

Collisions occur when $r = 1$ and $p_r < 0$. During an elastic hard-sphere collision, the values of p_θ and p_ϕ remain the same, and $p_r \rightarrow -p_r$. This ensures that the angle of incidence equals the angle of reflection, and the kinetic energy is conserved during collisions. We consider the collisions to occur instantaneously.

Our initial conditions yield periodic states whose trajectories are symmetric under reflections about the x axis, meaning that for every point (r, θ) on a periodic trajectory, there is a corresponding point $(r, -\theta)$ on that trajectory. This is easily seen by starting from the same initial conditions as described above, but with time reversed, that is, $r(0) = 1$, $\theta(0) = 0$, $\phi(0) = 0$, $p_r(0) \rightarrow -p_r(0)$, $p_\theta(0) \rightarrow -p_\theta(0)$, and $p_\phi(0) \rightarrow -p_\phi(0)$. Because $p_r(0)$ is now negative, the free sphere collides with the fixed sphere immediately after the free sphere is released, and this collision reverses the sign of $p_r(0)$ while leaving $p_\theta(0)$ and $p_\phi(0)$ the same. After this collision, we now have initial conditions that are symmetric about the x

axis relative to the original initial conditions. Thus, the symmetry of the initial position coupled with time reversal symmetry and hard-sphere collisions ensures that trajectories will be symmetric about the x axis. We have not investigated initial conditions that yield non-symmetric states.

For a state to be periodic, the free sphere must return to its initial position and momentum, and the time required for this to happen is defined as the period T of the motion. Once the initial momenta have been identified for a periodic state, we characterize the state using the same mode descriptors (m, n, p) that we use to classify the small-amplitude periodic modes, with $p = 1$ for in-phase modes and $p = 2$ for out-of-phase modes, as follows:

If $p_\theta(0)$ and $p_\phi(0)$ have the same sign, then we set $p = 1$ to reflect that the orbital and spin motions are initially in phase. To reflect the dominant role of orbital motion in this case, we define the rocking number n as the number of times that the sign of θ changes from negative to positive during each period. We define the bouncing number m as the number of hard-sphere collisions with the fixed sphere during each period, counting the final collision at time $t = T$ but not counting the initial contact at time $t = 0$. For these conditions, the mode designation is $(m, n, 1)$.

If $p_\theta(0)$ and $p_\phi(0)$ have opposite signs, then we set $p = 2$ to reflect that the orbital and spin motions are initially out of phase. To reflect the dominant role of spin motion in this case, we define the rocking number n as the number of times that the sign of β changes from negative to positive during each period. The angle β offers a more reliable indicator of spin oscillations than ϕ because, when $\beta = 0$, the magnetic moment of the free sphere points in the direction of the local magnetic field, so a sign change in β means that the magnetic moment now points to the other side of the local magnetic field. The magnetic torque acts to rotate the magnetic moment back into alignment with the field. We define the bouncing number m as before. For these conditions, the mode designation is $(m, n, 2)$.

If m and n have a common factor other than 1, then mode (m, n, p) is a duplicate of an irreducible mode $(m/k, n/k, p)$, where k is the greatest common factor of m and n . For example, for mode $(4, 2, 1)$, $m = 4$ and $n = 2$ have a greatest common factor of 2, and this mode is therefore a duplicate of the irreducible mode $(2, 1, 1)$. Indeed, the $(4, 2, 1)$ has the same energy as and twice the period of $(2, 1, 1)$, and simply executes the motion of $(2, 1, 1)$ twice. Irreducible modes (m, n, p) are those for which m and n have no common factors other than 1. To maximize the number of irreducible modes found in our finite-amplitude simulations, we give first preference to prime numbers and second preference to odd numbers in selecting values of m , while striving for even spacing of values of m on a logarithmic scale.

Table I lists the values of m considered, together with the number N_1 of in-phase ($p = 1$) modes and the num-

ber N_2 of out-of-phase ($p = 2$) modes found for each bouncing number m , for a total of 144 in-phase modes and 1353 out-of-phase modes, and a grand total of 1497 modes found. Also listed in Table I are the number n_1 of irreducible in-phase modes and the number n_2 of irreducible out-of-phase modes for each bouncing number m , obtained by omitting duplicates, for a total of 128 irreducible in-phase modes and 1115 irreducible out-of-phase modes, and a grand total of 1243 irreducible modes found. Of these, there are two anomalous mode descriptors, $(7, 2, 1)$ and $(11, 2, 1)$, each of which describes two distinct modes, each with its own energy, period, and motion. Each of the other mode descriptors pertains to a single mode.

For example, we find only one mode $(4, 2, 1)$, and it is a duplicate of the irreducible mode $(2, 1, 1)$ – we do not find another $(4, 2, 1)$ mode that is *not* a duplicate of mode $(2, 1, 1)$. Even though $(4, 2, 1)$ is a duplicate of another mode, it is the one-and-only $(4, 2, 1)$ mode, and therefore holds a place in the mode list for the purpose of analyzing trends in the mode energies and periods as functions of m , n , and p . For this reason, when performing such analyses below and in Ref. [16], we include both reducible and irreducible modes.

Table I. Numbers N_1 and N_2 of in-phase and out-of-phase modes found for each bouncing number m considered, and the numbers n_1 and n_2 of these modes that are unique, with values of m that are prime numbers in bold typeface.

m	N_1	N_2	n_1	n_2
1	0	20	0	20
2	0	17	0	9
3	1	13	1	10
4	1	15	1	7
5	1	18	1	14
6	1	20	1	5
7	3	21	3	19
9	2	27	2	19
11	4	30	4	29
13	4	32	4	30
15	3	35	3	21
19	5	42	5	41
23	5	49	5	49
27	5	50	4	34
31	10	53	10	52
39	10	64	6	40
47	11	70	11	70
55	13	82	10	61
63	7	94	4	56
79	13	93	13	93
95	14	106	12	80
111	8	128	5	82
127	12	121	12	121
157	11	153	11	153
TOTALS	144	1353	128	1115

V. NUMERICAL METHODS

In this section we describe our numerical methods for finding modes and periodic states within those modes. There are four specific methods we describe: magnet simulation, periodic state search, bifurcation search, and mode trace.

A. Magnet simulation

As described in detail in [15], we simulate a free magnet's interaction with a fixed magnet using fourth-order Runge-Kutta integration over the Hamiltonian equations described in [15]. For animation the algorithm runs until stopped by the user, but when searching for periodic states, we restrict the algorithm to iterate until a specified number of bounces m have occurred.

B. Periodic state search

As described in section IV, a periodic state is a set of initial conditions such that the free magnet returns to its initial position and momentum. Define $\mathbf{s}(t) = (p_\theta(t), p_\phi(t), E(t))$ to be a state's variables at time t and define an objective function

$$f(\mathbf{s}(0), t) = \|\mathbf{s}(t) - \mathbf{s}(0)\|_2 \quad (30)$$

(i.e. the ℓ^2 norm in parameter space of the difference in position and momentum). We consider a state to be periodic if $f(\mathbf{s}(0), t_m) < \epsilon$ where ϵ is a threshold value (we use 10^{-9} in our implementation).

We use the Nelder-Mead Simplex algorithm [18] to find minima of the function. Not all minima are periodic. A 2D projection of the objective function (30) is shown in figure 5. We can see that the function is complicated with non-uniformly spaced minima, so finding minima through a 2D gridded search would require a large amount of computation even for modest resolution. The following subsections describe our optimized search strategy.

C. Search for candidate bifurcations

This and the following subsection describe efficient algorithms to find periodic states by finding bifurcations from the finite-amplitude radial mode and then tracing out the mode in parameter space.

To find states that may be bifurcations from the finite-amplitude radial mode for a given number of bounces m we search at each point on a uniform grid of values $E(0) \in (-1/3, 0)$ with spacing 10^{-3} , and with $p_\phi(0) = 10^{-3}$, $r(0) = 1$, and $\theta(0) = \phi(0) = p_\theta(0) = 0$. We vary only p_θ and E , holding all other state variables constant, to ensure that the periodic state search doesn't pull the state back to the finite-amplitude radial mode. At each

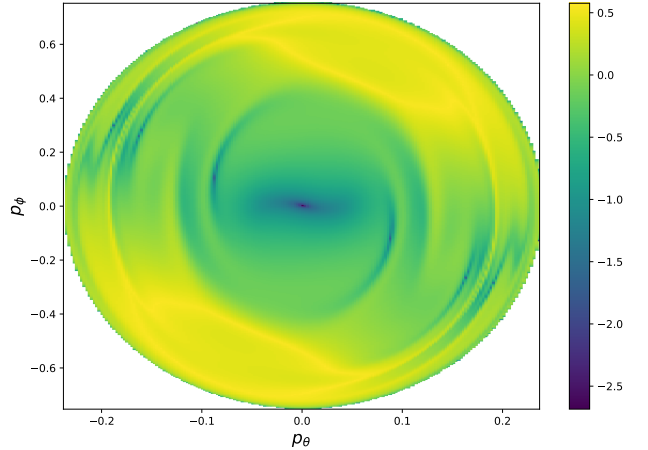


Figure 5. Plot of $\log f(\mathbf{s}(0), t)$ (see Eq. (30)) for values of p_θ and p_ϕ when the energy of the system is -0.05 and the number of bounces is 3. The colorbar gives the function value. The circular region is where valid values of the two variables are allowed based on Eqs. (??) and (??).

grid point, if the periodic state search finds a periodic minimum within 1000 iterations then we have found a candidate bifurcation with initial conditions $\mathbf{s}(0)$.

In practice, we sometimes find candidate bifurcations that meet our periodicity criterion but are not true bifurcations. This especially occurs at low energy since the free magnet is moving very little. One approach to ensuring that these states don't get reported as true bifurcations would be to normalize ϵ with a factor dependent on total movement of the magnet, but this could quickly lead to floating point underflow. Instead, we wait until after tracing a mode (see next step) before declaring a candidate bifurcation as a true bifurcation.

D. Mode trace

Once we have found a candidate bifurcation we trace out the mode in parameter space (see Fig. 6) starting with the state s_0 found by the bifurcation search and finding subsequent states s_1, s_2, \dots, s_k . To find s_1 we do a periodic state search from $s'_1 = s_0 + \mathbf{v}_1$ where $\mathbf{v}_1 = (p_{\theta,0}, p_{\phi,0}, 0)$. $p_{\theta,0}$ and $p_{\phi,0}$ are the p_θ and p_ϕ values for state s_0 , respectively. If the search finds a periodic state s_1 we continue and look for s_2 . For $i \neq 0$, to find s_{i+1} we search from $s'_{i+1} = s_i + \mathbf{v}_{i+1}$ where $\mathbf{v}_{i+1} = (p_{\theta,i} - p_{\theta,i-1}, p_{\phi,i} - p_{\phi,i-1}, E_i - E_{i-1})$ and if the search yields a periodic minimum we call it s_{i+1} . This approach uses principles of both the Euler method and finite differences, where we use finite differences to approximate the derivative for the Euler step, but then we use the periodic state search to refine our Euler guess, moving it onto the true mode trace curve. The search ends when the periodic state search fails.

After tracing the states of the mode, we look at the

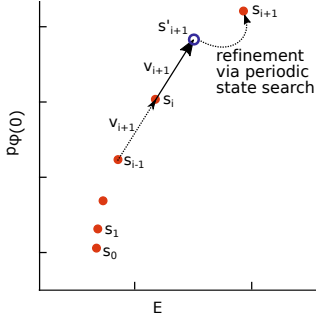


Figure 6. Approach to tracing the states in a given mode. p_θ and \mathbf{v}_1 are omitted and distances between states are exaggerated for clarity. See Fig. 12 for states with $m = 1$.

last state found s_k . If $p_{\phi,k} > 10^{-3}$ then we consider the mode legitimate. Otherwise, the candidate bifurcation is spurious and we discard it.

E. Implementation

We have two implementations of the magnet simulation algorithm. The first is in Javascript and is used in the *MagPhyx* software to visualize magnet interactions. This implementation provides not only an animation available on the *MagPhyx* website, but also the path traces shown in this paper (e.g. Fig. 18). The second implementation is done in C++ for performance and is used in searching for periodic states.

The periodic state search is implemented in C++ and uses the Gnu Scientific Library's [19] implementation of the Simplex algorithm. The search for candidate bifurcations and mode tracing are both done in Python, calling the C++ subroutine to search for periodic states.

MagPhyx simulation software [20], *MagPhyx* code [21], data visualizations [22], and C++ code [23] are all publicly available.

VI. TRAJECTORIES

In this section, we describe the results of our findings for finite-amplitude states.

Figure 7 is a plot of $|p_\phi(0)|$ vs. E showing periodic out-of-phase states ($p = 2$, filled circles) with bouncing number $m = 1$ and rocking numbers $n = 1, 2, 3, \dots$. Families of states are labeled by their mode descriptors (m, n, p) . States within each family differ in the amplitude of their angular motion but otherwise behave similarly. Each family has a continuum of states with a continuous range of values of $|p_\phi(0)|$ and E ; only a discrete subset of this continuum is shown in Fig. 7. For $m = 1$, only out-of-phase states ($p = 2$) are found, with $p_\phi(0)$ and $p_\theta(0)$ having opposite signs. For each state with positive initial spin momentum $p_\phi(0)$, there is a corresponding state with the same energy and negative initial

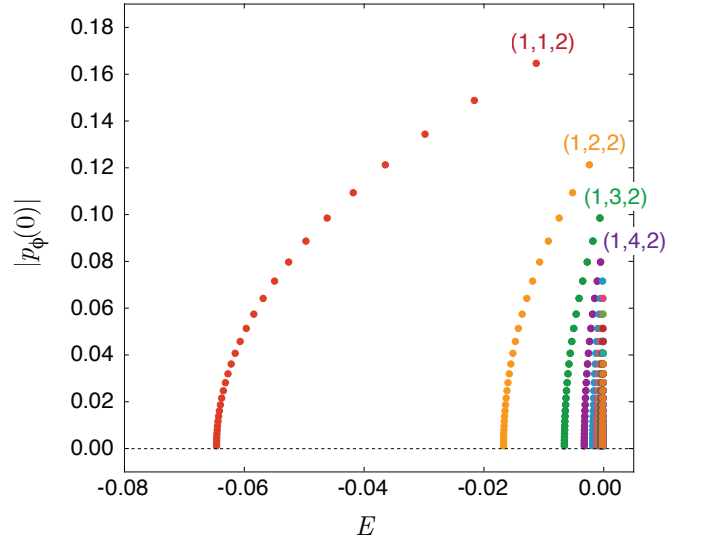


Figure 7. Initial spin momentum $|p_\phi(0)|$ vs. energy E for finite-amplitude out-of-phase periodic states ($p = 2$, filled circles) with bouncing number $m = 1$ and rocking numbers $n = 1, 2, 3, \dots$. Each mode (m, n, p) has a family of states with different paired values of E and $|p_\phi(0)|$, starting at a threshold energy $E = E_{mnp}$ with $|p_\phi(0)| \rightarrow 0$, and with $|p_\phi(0)|$ increasing with increasing $E > E_{mnp}$.

spin momentum $-p_\phi(0)$.

Figure 7 illustrates how the finite-amplitude radial mode bifurcates into modes with angular motion. In the finite-amplitude radial mode, the magnetic moments of the two spheres point in the $+x$ direction and the free sphere travels along the $+x$ axis, with its south pole bouncing repeatedly against the north pole of the fixed sphere – there is no spin or orbital motion. As the energy increases, modes (m, n, p) first appear with infinitesimal angular motion, $p_\phi(0) \rightarrow 0$ and $p_\theta(0) \rightarrow 0$. We designate this minimum-energy state as the threshold state, with energy E_{mnp} and period T_{mnp} . As the energy increases beyond this threshold for mode (m, n, p) , the amplitude of the angular motion increases. Thus, the threshold energy E_{mnp} and period T_{mnp} correspond to finite-amplitude radial motion and infinitesimal-amplitude angular motion.

The lowest-energy mode in Fig. 7 is the $(1, 1, 2)$ mode. In this mode, the free sphere completes one bounce ($m = 1$) and one rocking cycle ($n = 1$) per period, with spin and orbital oscillations that are out of phase with each other ($p = 2$). Figure 8 shows a series of *MagPhyx* snapshots of the motion of the free sphere in this mode during one period of the motion, and Fig. 9 shows how the amplitude of the angular motion increases with increasing energy. Table II gives the corresponding values of E , T , and $p_\phi(0)$, and refers to online *MagPhyx* visualizations of these states.

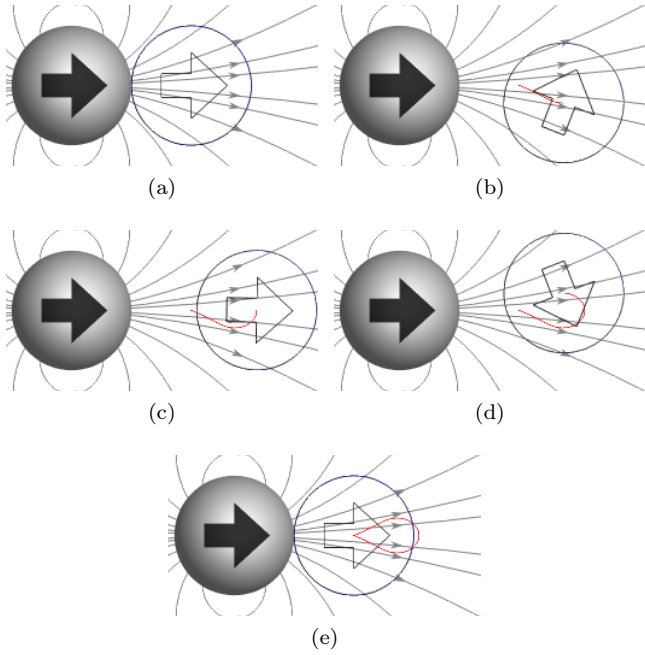


Figure 8. *MagPhyx* snapshots of mode (1,1,2) with $p_\phi(0) = 0.1645$. In this mode, the spin and orbital motions are out of phase with each other, with spin motion dominating over orbital motion; the magnetic displacement angle covers a large range $-78^\circ < \beta < +78^\circ$ while the orbital position angle is restricted to the narrow range $-6.2^\circ < \theta < +6.2^\circ$.

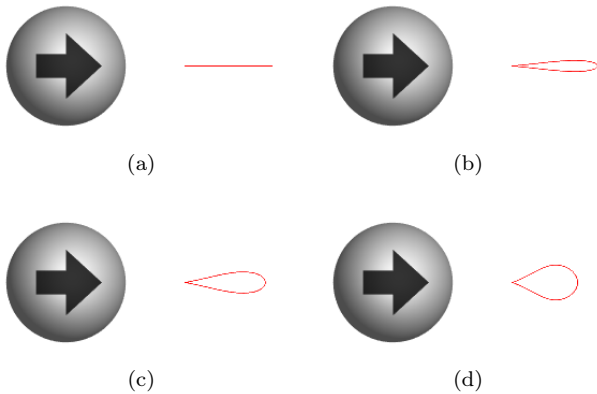


Figure 9. *MagPhyx* trajectories for mode (1,1,2) with $p_\phi(0) = 0.0010$ (a), 0.0512 (b), 0.0983 (c), and 0.1645 (d). Frame (d) replicates the trajectory shown in Fig. 8.

The second-lowest energy mode in Fig. 7 is the (1, 2, 2) mode, which exhibits two rocking cycles per period ($n = 2$) but is otherwise similar to the (1, 1, 2) mode. The third-lowest energy mode is the (1, 3, 2) mode, which exhibits three rocking cycles per period. Shown in Fig. 10 are *MagPhyx* trajectories for these three modes. Other one-bounce modes in Fig. 7 behave similarly, differing only in the number of rocking cycles. All $m = 1$ modes have single-passage trajectories, meaning that the free sphere passes along the trajectory just once per period.

For bouncing number $m = 2$, the plot of $|p_\phi(0)|$ vs. E is similar to Fig. 7, except that it has more states and lower-energy states. The lowest of these is mode (2,1,2), whose trajectory is shown in Fig. 11(a). In this mode, the free sphere bounces twice against the fixed sphere during each period of the motion, with both bounces occurring at the same place, $\theta = \phi = 0$, and with $p_\theta > 0$ for one bounce and $p_\theta < 0$ for the other. The free sphere has a double-passage trajectory, that is, it passes twice along the same path during each period of the motion, once in each direction.

It is also instructive to consider $m = 2$ modes with $n > 1$. Modes (2,2,2) and (2,4,2) are duplicates of modes (1,1,2) and (1,2,2) shown in Figs. 10(a,b). Modes (2,3,2) and (2,5,2) are unique, and are shown in Figs. 11(b,c). All unique $m = 2$ modes have double-passage trajectories, whereas $m = 1$ modes (and their $m = 2$ duplicates) have single-passage trajectories.

Table II. List of modes illustrated in this paper, together with demo numbers for associated *MagPhyx* visualizations [17].

Figure	Mode	E	T	$p_\phi(0)$	Demo
2	(1,0,0)	-0.0988	3.98	0.0000	1
3	(0,1,1)	-0.2900	14.76	0.0413	11
4	(0,1,2)	-0.2900	3.15	-0.0832	12
8	(1,1,2)	-0.0112	5.85	0.1645	24
9(a)	(1,1,2)	-0.0646	6.16	0.0010	25
9(b)	(1,1,2)	-0.0596	6.14	0.0512	26
9(c)	(1,1,2)	-0.0461	6.09	0.0983	27
9(d)	(1,1,2)	-0.0112	5.85	0.1645	28
10(a)	(1,1,2)	-0.0461	6.09	0.0983	29
10(b)	(1,2,2)	-0.0074	20.60	0.0983	30
10(c)	(1,3,2)	-0.0006	45.07	0.0983	31
11(a)	(2,1,2)	-0.1306	4.31	0.0983	32
11(b)	(2,3,2)	-0.0176	24.18	0.0983	33
11(c)	(2,5,2)	-0.0025	62.82	0.0983	34
13(a)	(3,1,2)	-0.0606	3.90	0.1819	35
13(b)	(3,2,2)	-0.0291	9.49	0.1819	36
13(c)	(3,4,2)	-0.0121	28.77	0.1211	37
13(d)	(3,5,2)	-0.0118	43.29	0.1092	38
13(e)	(3,7,2)	-0.0049	82.66	0.0795	39
13(f)	(3,8,2)	-0.0058	107.38	0.0573	40
14	(3,1,1)	-0.0068	123.08	0.0214	41
15(a)	(4,1,2)	-0.0861	3.64	0.1819	42
15(b)	(4,3,2)	-0.0300	14.45	0.1645	43
15(c)	(4,5,2)	-0.0186	33.00	0.1211	44
15(d)	(4,1,1)	-0.0186	64.14	0.0640	45
15(e)	(4,7,2)	-0.0067	60.86	0.0885	46
15(f)	(4,9,2)	-0.0082	101.92	0.0975	47
17(a)	(79,1,1)	-0.1864	20.06	0.0714	48
17(b)	(79,4,1)	-0.2218	67.24	0.0456	49
17(c)	(79,13,1)	-0.0663	414.73	0.0280	50
17(d)	(79,24,1)	-0.0109	2350.80	0.0159	51
18(a)	(79,33,2)	-0.1650	126.45	0.0795	52
18(b)	(79,49,2)	-0.1046	218.23	0.1092	53
18(c)	(79,55,2)	-0.0859	257.55	0.1092	54
18(d)	(79,57,2)	-0.0877	270.84	0.0983	55
18(e)	(79,63,2)	-0.0744	315.45	0.0885	56
18(f)	(79,74,2)	-0.0659	412.86	0.0512	57

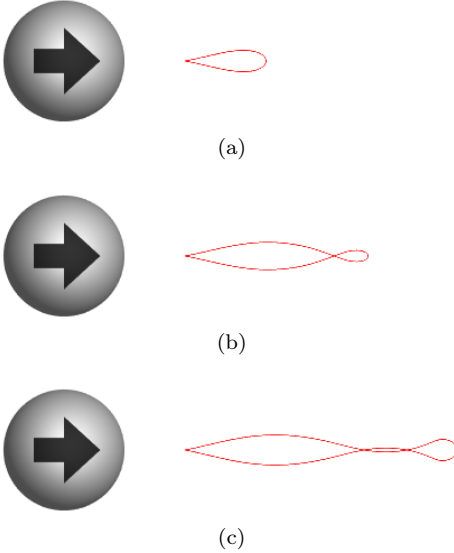


Figure 10. Single-passage *MagPhyx* trajectories for modes $(1,1,2)$ (a), $(1,2,2)$ (b), and $(1,3,2)$ (c), all with $p_\phi(0) = 0.0093$. Frame (a) replicates the trajectory shown in Fig. 9(c).

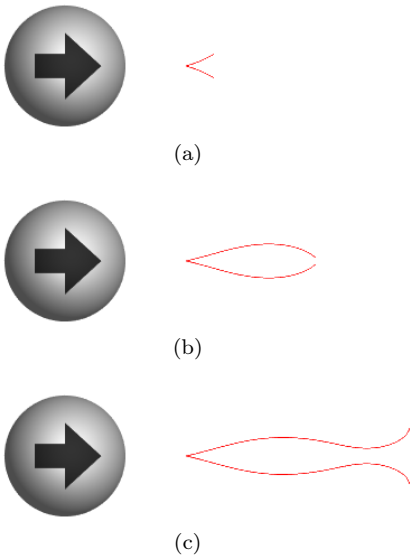
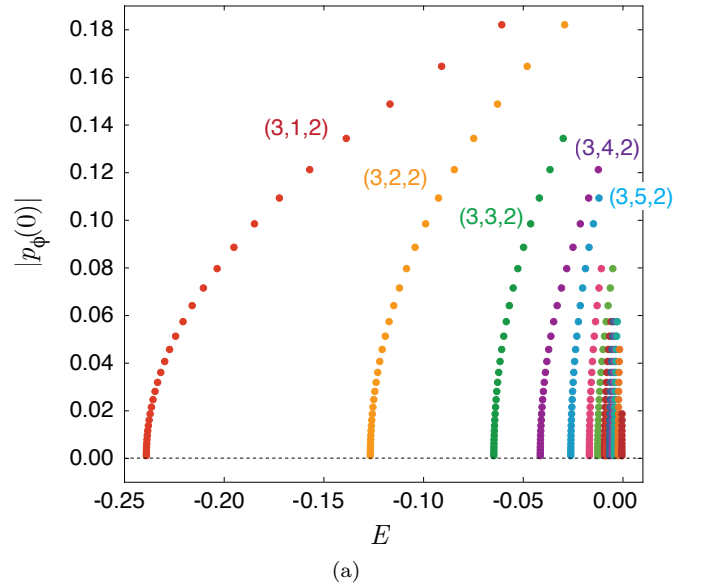


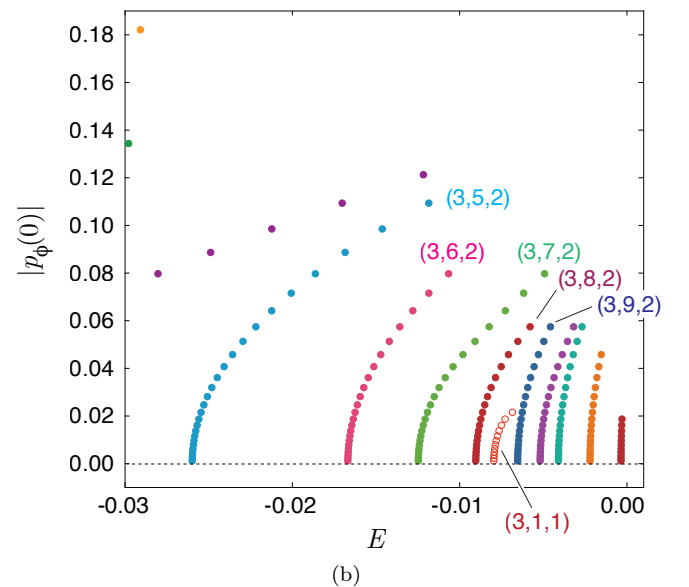
Figure 11. Double-passage *MagPhyx* trajectories for modes $(2,1,2)$ (a), $(2,3,2)$ (b), and $(2,5,2)$ (c), all with $p_\phi(0) = 0.0093$.

For $m = 2$ modes with $n = 1, 5, 9$, etc., the two sides of the trajectory diverge at the end, like a vase, with the number of lobes in the trajectory increasing with increasing n [Figs. 11(a,c)]. For $n = 3, 7, 11$, etc., the two sides of the trajectory approach but do not touch each other at the end, like a pair of open tweezers [Fig. 11(b)].

Bouncing number $m = 3$ is the smallest bouncing number that has in-phase states ($p = 1$). Figure 12 shows $|p_\phi(0)|$ vs. E for $m = 3$, with out-of-phase states ($p = 2$) denoted by closed circles and in-phase states ($p = 1$) denoted by open circles. As E increases, there are eight out-of-phase modes (for $n = 1, 2, \dots, 8$) before the



(a)



(b)

Figure 12. Initial spin momentum $|p_\phi(0)|$ vs. energy E for finite-amplitude out-of-phase periodic states ($p = 2$, filled circles) and in-phase periodic states ($p = 1$, open circles) with bouncing number $m = 3$ and rocking numbers $n = 1, 2, 3, \dots$, with some mode families (m, n, p) indicated. Frame (a) shows the entire range of energies, and frame (b) is a closeup of high-energy states.

first in-phase mode $(3,1,1)$ is seen. Of these eight modes, $(3,3,2)$ is a duplicate of $(1,1,2)$ and $(3,6,2)$ is a duplicate of $(1,2,2)$. Single-passage *MagPhyx* trajectories for the remaining six out-of-phase modes are shown in Fig. 13.

The first and only in-phase mode for $m = 3$ is the $(3,1,1)$ mode, which executes one cycle of in-phase rocking motion while bouncing three times. Shown in Fig. 14 are snapshots of its single-passage trajectory at different points during one period of its motion. Note that, in this mode, the free dipole is generally aligned closely with

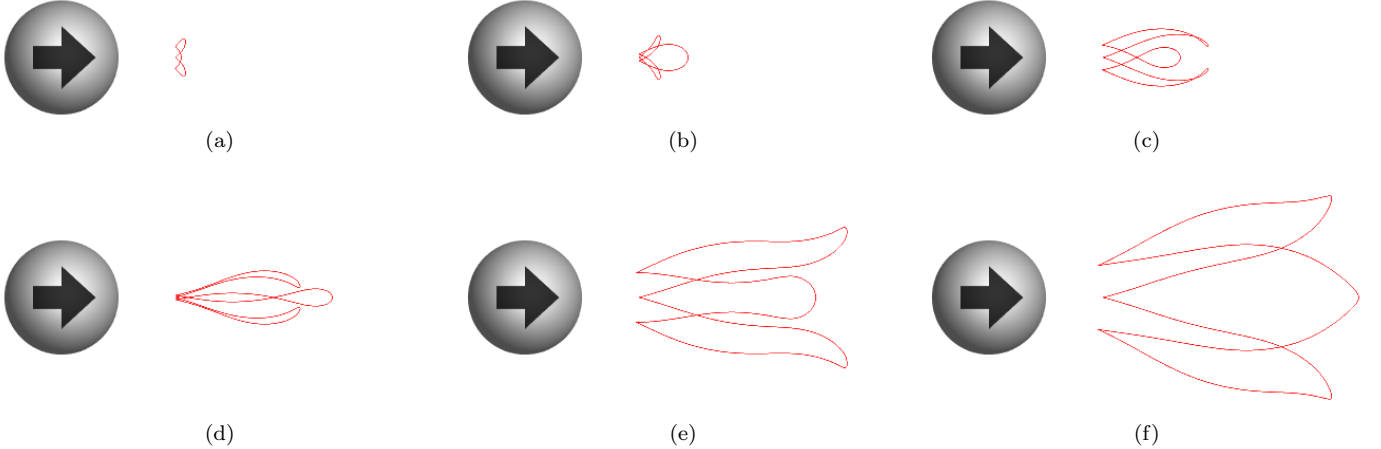


Figure 13. Single-passage *MagPhyx* trajectories for irreducible modes (3,1,2), (3,2,2), (3,4,2), (3,5,2), (3,7,2), and (3,8,2).

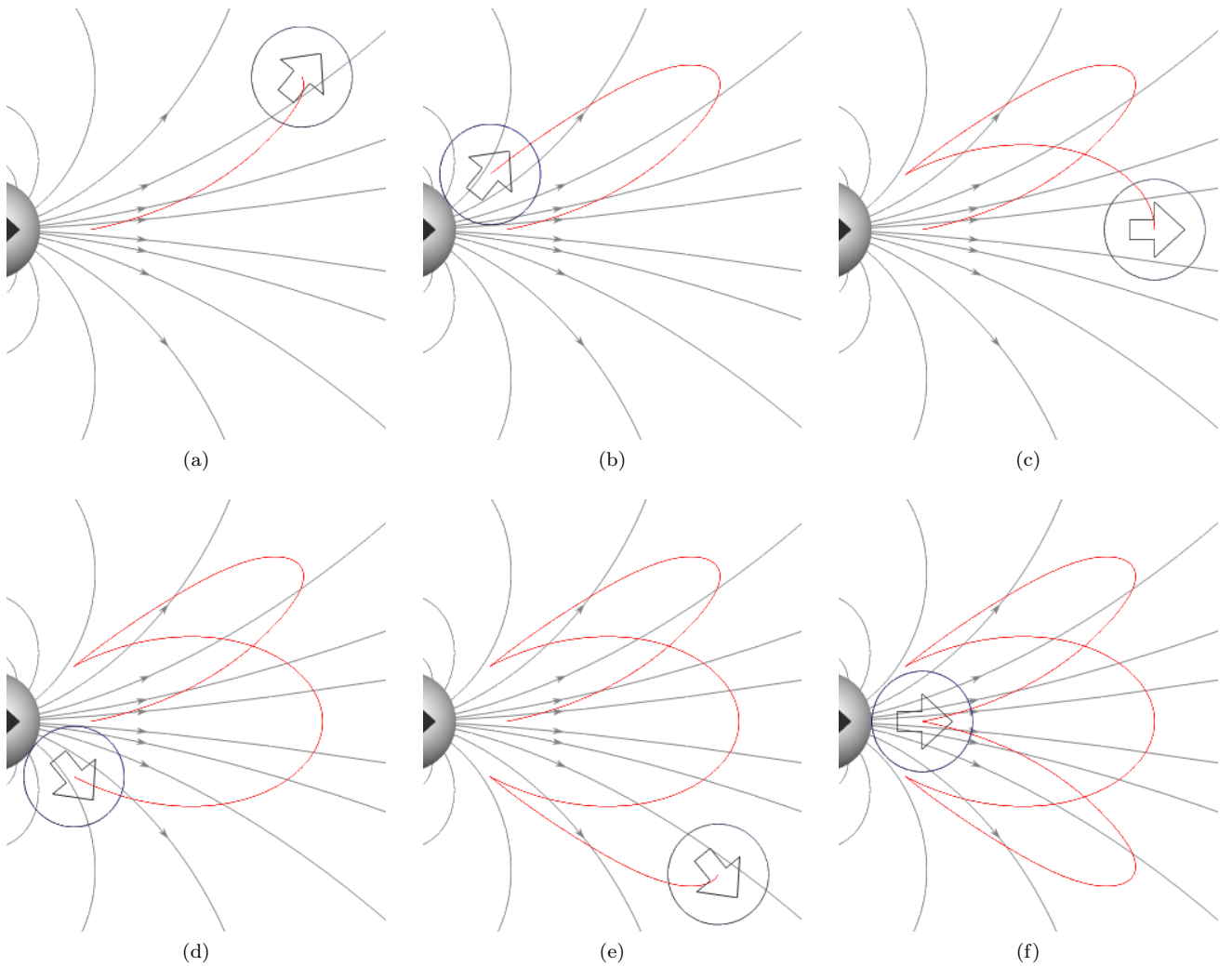


Figure 14. *MagPhyx* snapshots of mode (3,1,1) with $p_\phi(0) = 0.0214$. In this mode, the spin and orbital motions are in phase with each other, with orbital motion dominating over spin motion; the orbital position angle covers a large range $35^\circ < \theta < +35^\circ$ while the magnetic displacement angle is restricted to $11^\circ < \beta < +11^\circ$.

the magnetic field, and the oscillations in θ and ϕ are in phase.

For bouncing number $m = 4$, the plot of $|p_\phi(0)|$ vs. E is similar to Fig. 12, and again features just one in-phase mode, (4,1,1). Shown in Fig. 15 are *MagPhyx* double-passage trajectories for the first few irreducible $m = 4$ modes.

Irreducible modes with nonzero angular motion and odd bouncing numbers m have single-passage trajectories, and those with even bouncing numbers have double-passage trajectories. This is a consequence of the symmetry of the initial conditions and of the hard-sphere collisions: The free sphere starts at $(r, \theta, \phi) = (1, 0, 0)$, just after leaving contact with the fixed sphere, with nonzero $p_\theta(0)$ and $p_\phi(0)$. Consequently, the free sphere is launched at a nonzero angle α relative to the $+x$ axis. For the trajectory to be periodic, the final collision must be at the starting point $(r, \theta, \phi) = (1, 0, 0)$, at the end of one period of the motion. This collision is a hard-sphere collision, so the angle of approach to the final collision must be $-\alpha$. Thus, for $m = 1$, the free sphere cannot retrace its steps as it completes one period, and must return to its starting point along a different path. For $m = 3$, the sphere must bounce once in the first quadrant and once in the fourth quadrant before returning to its initial position for the final bounce. And so on for $m = 5, 7, \dots$. For $m = 2$, the free sphere must retrace its steps so that the first collision, at time $t = T/2$, occurs at $(r, \theta, \phi) = (1, 0, 0)$, so that it can return to this position at time $t = T$. For $m = 4$, the sphere must bounce two more times, once in the first quadrant and once in the fourth quadrant. And so on for $m = 6, 8, \dots$.

To illustrate the richness and variety of our periodic finite-amplitude trajectories, we consider bouncing number $m = 79$. Figure 16 shows $|p_\phi(0)|$ vs. E for the 13 in-phase modes and 93 out-of-phase modes found for $m = 79$, all of which are irreducible (Table I).

Figure 17 shows single-passage trajectories for four of these in-phase modes, which resemble Spirograph paths [24]. Panel (a) shows mode (79,1,1), for which the free sphere bounces 79 times while completing one cycle of orbital oscillation, starting at $\theta = 0$ initially and passing in turn through the values $\theta = 71^\circ, 0, -71^\circ$ and 0 at times $t = T/4, T/2, 3T/4$, and T to complete one period of the motion. The free sphere remains very close to the fixed sphere and collides with it frequently, giving a short overall period, $T = 20.06$ (Table II). At first glance, the trajectory looks like a circular arc subtending an angle of 142° , but at screen resolutions, one can just discern a subtle scalloped substructure, with 79 scallops corresponding to the 79 bounces. Panel (b) shows mode (79,4,1), for which the free sphere bounces 79 times during four cycles of orbital oscillation. The amplitude of the radial motion is larger and the collisions are less frequent than for (79,1,1), giving an easily discerned substructure and a longer overall period $T = 67.24$ (Table II). Modes (79,13,1) and (79,24,1), shown in panels (c) and (d), have yet greater radial amplitudes, less frequent

collisions, and longer periods.

Shown in Fig. 18 are trajectories for six out-of-phase modes for $m = 79$. In contrast with the in-phase modes, which have trajectories that are similar except for their radial and orbital amplitudes, the trajectories for the out-of-phase modes show great variety. The six modes shown represent a small fraction of the possible trajectories, and were selected to illustrate their folded textures, complex symmetries, and breathtaking beauty. The time-development of these trajectories is particularly fascinating; the symmetry of the final trajectory sometimes emerges only in the late stages of the motion, and the order of appearance of the various traces that make up the whole seems virtually impossible to predict. Yet each of these trajectories is a single, continuous, closed path that crosses over itself many times before meeting up with its starting point to complete one period T of the motion, and retraces its steps during each subsequent period of the motion. See Table II for information on freely available online *MagPhyx* visualizations of the time development of these states.

Figures 7, 12, and 16 indicate that the threshold energy $E_{m,1,2}$ decreases with increasing m , with $E_{m,1,2} \rightarrow 0$ as $m \rightarrow \infty$. This limit satisfies $m \gg n$, the condition for small-amplitude modes, for which Eqs. (28) and (29) are valid. In this limit, the amplitudes of the radial, orbital, and spin motions are all infinitesimal, the free sphere remains very near its stable equilibrium position, and collides frequently with the fixed sphere.

VII. CONCLUSIONS

We investigate the periodic motion of a free uniformly magnetized sphere subject to the fields of a second, fixed sphere, when the free sphere is located initially at its stable equilibrium point, $(r, \theta, \phi) = (1, 0, 0)$. We show that these initial conditions produce a rich spectrum of symmetric periodic modes. Taking a cue from our small-amplitude analysis, we characterize these modes by their bouncing numbers m , rocking numbers n , and phases p .

We find 1,243 distinct periodic modes numerically, each with a threshold energy E_{mnp} and an associated period T_{mnp} , and each with a family of states with differing amplitudes of angular motion. One of these is mode $(m, n, p) = (157, 580, 2)$, with $T_{mnp} = 11,298$, which requires about 16,000 Runge-Kutta time steps to integrate. *MagPhyx* visualizations of the modes that are illustrated in this paper are freely available online (Table II). In a companion paper, we investigate scaling relationships for E_{mnp} and T_{mnp} [16].

We show that irreducible modes with angular motion and odd bouncing numbers m traverse their trajectories just once per period, and show that irreducible modes with nonzero angular motion and even bouncing numbers traverse their trajectories twice during one period of the motion, once in each direction.

Of interest are the stability of the 1,243 modes. We

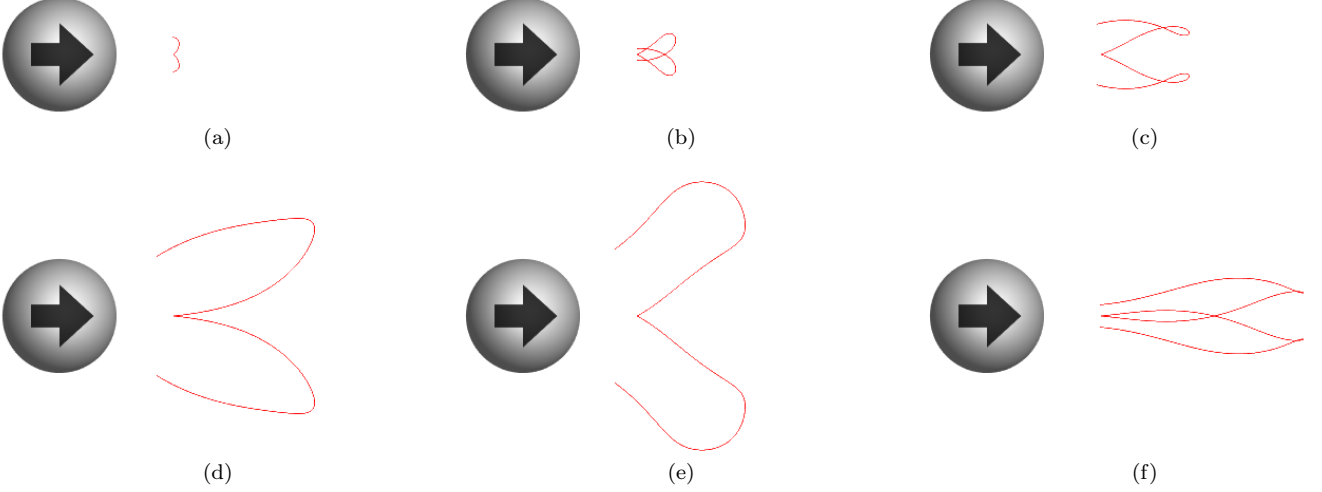


Figure 15. Double-passage *MagPhyx* trajectories for irreducible modes $(4,1,2)$, $(4,3,2)$, $(4,5,2)$, $(4,1,1)$, $(4,7,2)$, and $(4,9,2)$.

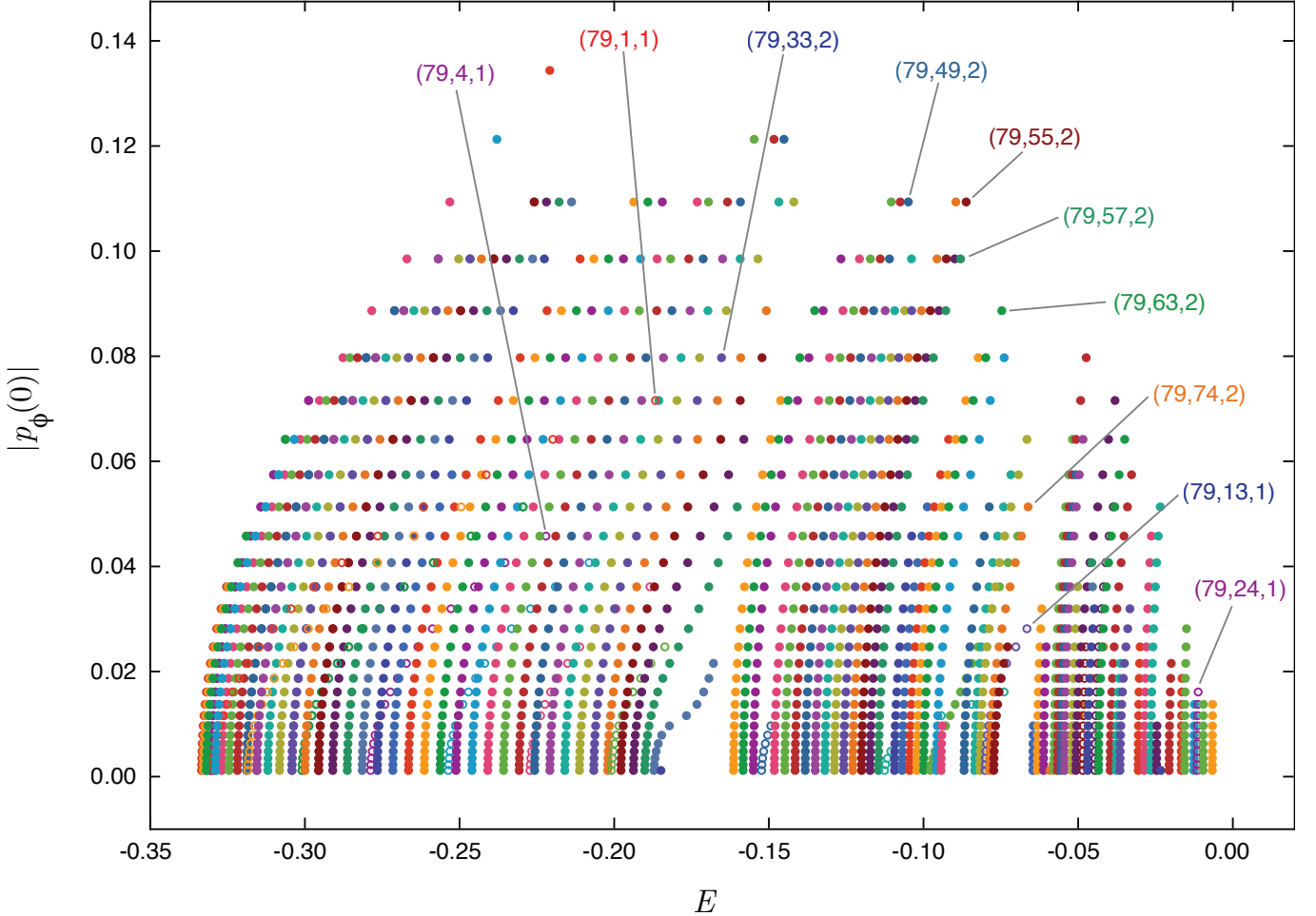


Figure 16. Initial spin momentum $|p_\phi(0)|$ vs. energy E for finite-amplitude out-of-phase periodic states ($p = 2$, filled circles) and in-phase periodic states ($p = 1$, open circles) with bouncing number $m = 79$ and various rocking numbers n . States illustrated in Figs. (17) and (18) are labeled by their mode descriptors (m, n, p) .

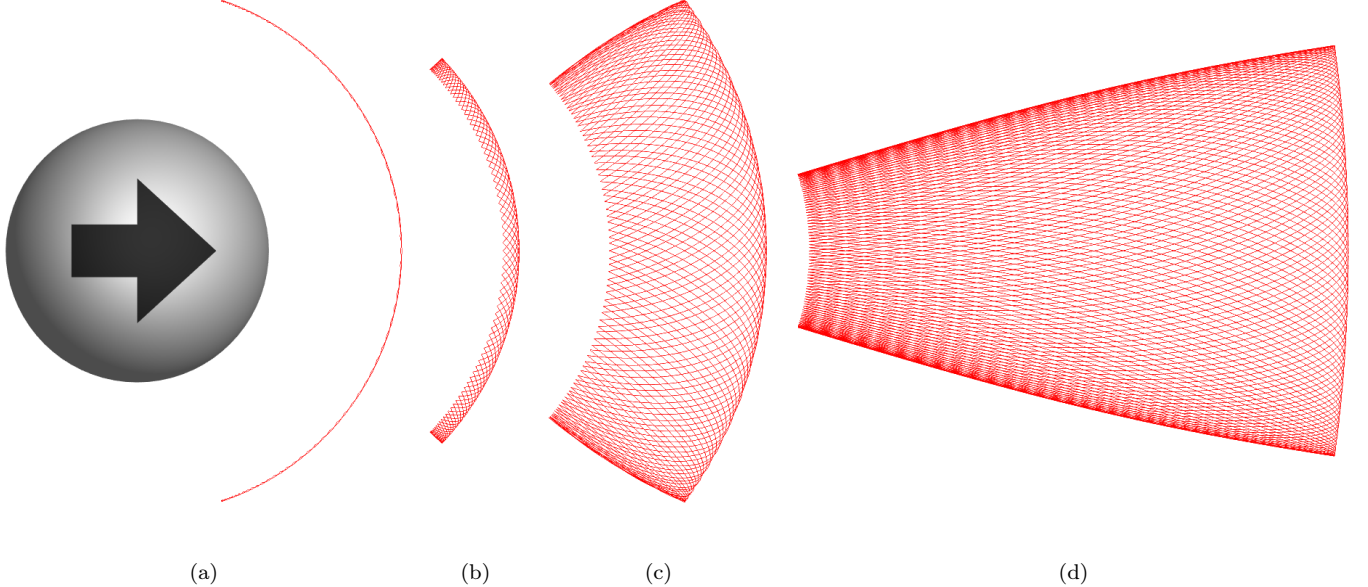


Figure 17. Single-passage in-phase *MagPhyx* trajectories for modes $(79,1,1)$, $(79,4,1)$, $(79,13,1)$, and $(79,24,1)$, shown respectively in panels (a), (b), (c), and (d). The length scales for all four trajectories are the same, and are set by the size of the grey (fixed) sphere.

have noticed that, when our simulations are allowed to run over several periods, the trajectory eventually diverges from the periodic trajectory for some modes, and remains on track for other modes. We would like to compute Lyapunov exponents for the various modes to discover which modes are stable, and why. We would also like to characterize the initial conditions generally resulting in periodic, quasiperiodic, and chaotic motion of the system. We are particularly interested in investigating

the behavior of the free sphere when located initially at the unstable equilibrium point $(r, \theta, \phi) = (1, \pi/2, \pi)$.

Our search for periodic states excludes high-energy periodic states for which the free sphere circumnavigates the fixed sphere. We have found such periodic states when the free sphere is constrained to remain in frictionless contact with the fixed sphere at all times [13]. We expect such states to also exist when this constraint is removed, and we are interested in searching for such states.

-
- [1] S. Qu, “The Zen Gallery.” <http://zenmagnets.com/gallery/> (accessed 20-May-2019), 2014.
- [2] B. F. Edwards, “Educational Value of Neodymium Magnet Spheres: Expert Report in the matter of Zen Magnets, LLC, CPSC Docket No. 12-2, Appendix D, 10/20/2014 (Redacted).” <https://drive.google.com/file/d/0Bw7DdocNZGQgWThTb3VvUHYza2s/view> (accessed 20-May-2019), 2014.
- [3] B. F. Edwards, “Educational Value of Neodymium Magnet Spheres: Expert Report in the matter of Zen Magnets, LLC, CPSC Docket No. 12-2, 10/20/2014 (Redacted).” <https://drive.google.com/file/d/0Bw7DdocNZGQgWThTb3VvUHYza2s/view> (accessed 20-May-2019), 2014.
- [4] J. Weis and D. Levesque, “Chain formation in low density dipolar hard spheres: a Monte Carlo study,” *Physical Review Letters*, vol. 71, no. 17, p. 2729, 1993.
- [5] A. Clarke and G. Patey, “Ground state configurations of model molecular clusters,” *The Journal of Chemical Physics*, vol. 100, no. 3, pp. 2213–2219, 1994.
- [6] R. Messina, L. A. Khalil, and I. Stanković, “Self-assembly of magnetic balls: From chains to tubes,” *Physical Review E*, vol. 89, no. 1, p. 011202, 2014.
- [7] C. L. Hall, D. Vella, and A. Goriely, “The mechanics of a chain or ring of spherical magnets,” *SIAM Journal on Applied Mathematics*, vol. 73, no. 6, pp. 2029–2054, 2013.
- [8] D. Vella, E. du Pontavice, C. L. Hall, and A. Goriely, “The magneto-elastica: from self-buckling to self-assembly,” *Proceedings of the Royal Society A: Mathematical, Physical and Engineering Sciences*, vol. 470, no. 2162, p. 20130609, 2014.
- [9] N. Vandewalle and S. Dorbolo, “Magnetic ghosts and monopoles,” *New Journal of Physics*, vol. 16, no. 1, p. 013050, 2014.
- [10] J. Boisson, C. Rouby, J. Lee, and O. Doaré, “Dynamics of a chain of permanent magnets,” *EPL (Europhysics Letters)*, vol. 109, no. 3, p. 34002, 2015.
- [11] J. Schönke and E. Fried, “Stability of vertical mag-

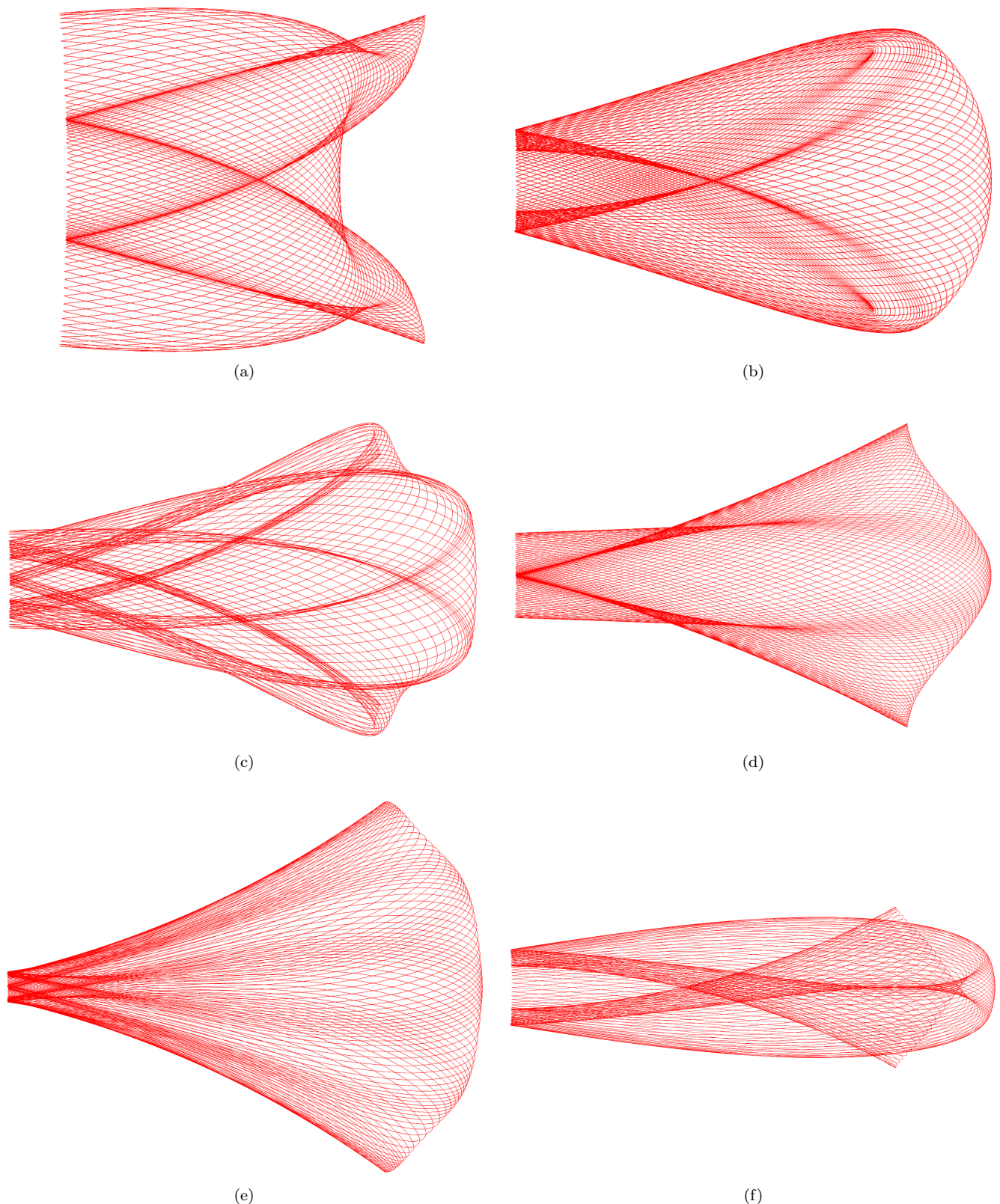


Figure 18. Single-passage out-of-phase *MagPhyx* trajectories for modes (79,33,2) “the owl” (a), (79,49,2) “the alien” (b), (79,55,2) “the vase” (c), (79,57,2) “the stingray” (d), (79,63,2) “the fan” (e), and (79,74,2) “the cigar” (f). See Table II for information on freely available online *MagPhyx* visualizations of the time development of these modes.

- netic chains,” *Proceedings of the Royal Society A: Mathematical, Physical and Engineering Sciences*, vol. 473, no. 2198, p. 20160703, 2017.
- [12] G. L. Pollack and D. R. Stump, “Two magnets oscillating in each other’s fields,” *Canadian journal of physics*, vol. 75, no. 5, pp. 313–324, 1997.
- [13] B. F. Edwards and J. M. Edwards, “Periodic nonlinear sliding modes for two uniformly magnetized spheres,” *Chaos*, vol. 27, no. 5, 2017.
- [14] B. F. Edwards, D. M. Riffe, J. Ji, and W. A. Booth, “Interactions between uniformly magnetized spheres,” *American Journal of Physics*, vol. 85, no. 2, pp. 130–134, 2017.
- [15] B. F. Edwards and J. M. Edwards, “Dynamical interactions between two uniformly magnetized spheres,” *European Journal of Physics*, vol. 38, no. 1, p. 015205, 2016.
- [16] B. F. Edwards, B. A. Johnson, and J. M. Edwards, “Periodic bouncing modes for two uniformly magnetized spheres II: Scaling,” *Chaos*, 2019.
- [17] J. Edwards, “*MagPhyx* Visualization Software.” <http://edwardsjohnmartin.github.io/MagPhyx/> (accessed 12-June-2019), 2019.
- [18] J. A. Nelder and R. Mead, “A simplex method for function minimization,” *The computer journal*, vol. 7, no. 4, pp. 308–313, 1965.
- [19] B. Gough, *GNU Scientific Library Reference Manual - Third Edition*. Network Theory Ltd., 3rd ed., 2009.
- [20] <http://edwardsjohnmartin.github.io/MagPhyx>.
- [21] github.com/edwardsjohnmartin/MagPhyx.
- [22] [edwardsjohnmartin.github.io/MagPhyxP/vis/](https://github.com/edwardsjohnmartin/MagPhyxP/vis/).
- [23] github.com/edwardsjohnmartin/MagPhyxP.
- [24] D. Fisher, “Wikipedia: Spirograph.” <https://en.wikipedia.org/wiki/Spirograph> (accessed 25-July-2019), 2019.